Pathogenesis of Nephronophthisis Caused by ADAMTS9 Mutations

Yo Jun Choi

Department of Medical Science

The Graduate School, Yonsei University

Pathogenesis of Nephronophthisis Caused by ADAMTS9 Mutations

Yo Jun Choi

Department of Medical Science

The Graduate School, Yonsei University

Pathogenesis of Nephronophthisis Caused by ADAMTS9 Mutations

Directed by Professor Heon Yung Gee

The Doctoral Dissertation
submitted to the Department of Medical Science,
the Graduate School of Yonsei University
in partial fulfillment of the requirements for the degree of
Doctor of Philosophy

Yo Jun Choi

JUNE 2021

This certifies that the Doctoral Dissertation of Yo Jun Choi is approved.

Thesis Supervisor : Heon Yung Gee

Thesis Committee Member#1 : Min Goo Lee

Thesis Committee Member#2 : Jinwoong Bok

Thesis Committee Member#3: Seok Jun Moon

Thesis Committee Member#4: Hyuk Wan Ko

The Graduate School
Yonsei University

JUNE 2021

ACKNOWLEDGEMENTS

I would like to thank all the professors, colleagues, and lab members for their assistance in my doctoral course, especially Professor Heon Yung Gee. I also wish to express my sincere gratitude to my parents and family, especially Seon Hwa Oh, for their encouragement and assistance.

TABLE OF CONTENTS

LIST OF FIGURES

LIST OF TABLES

ABSTRACT

Pathogenesis of Nephronophthisis Caused by ADAMTS9 Mutations

Yo Jun Choi

Department of Medical Science
The Graduate School, Yonsei University

(Directed by Professor Heon Yung Gee)

Defects in primary cilia result in a group of heterogenous diseases called nephronophthisis-related ciliopathy (NPHP-RC). More than 90 genes have been reported as a monogenic recessive cause of NPHP-RC, which accounts for 50~60% of NPHP-RC cases. Whole exome sequencing analysis of individuals with NPHP-RC revealed ADAMTS9 as a novel renal ciliopathy gene in 4 patients with early-onset end-stage renal disease (ESRD) and NPHP with various extrarenal symptoms including short stature, deafness, and developmental delay. Although ADAMTS9 is known as a metalloprotease which cleaves the extracellular matrix component, we found that ADAMTS9 is located near the basal bodies of primary cilia during interphase. In addition, loss of ADAMTS9 resulted in shortened primary cilia and defective sonic hedgehog signaling. Functional study demonstrated that the identified four mutations (p.T65R, p.Q1525Hfs*60, p.C1024*, and p.S636F) disrupted the localization of ADAMTS9 near basal bodies. Knockout of Adamts9 in a renal tubular cell line resulted in defective lumen formation upon spheroid induction, which was rescued by overexpression of wild-type, but not mutant ADAMTS9. Knockdown of adamts9 in zebrafish recapitulated NPHP-RC phenotypes, including renal cysts and hydrocephalus. We also established ADAMTS9 knockout human induced pluripotent stem cells by

using CRISPR/Cas9 and differentiated into kidney organoid. We found ciliary defects in kidney organoid with deletion of ADAMTS9. These results indicate that the identified mutations in ADAMTS9 are pathogenic and that ADAMTS9 is required for the formation and function of primary cilia.

Key Words: nephronophthisis-related ciliopathy, nephronophthisis, ADAMTS9, metalloproteinase, kidney organoid, primary cilia.

Pathogenesis of Nephronophthisis Caused by ADAMTS9 Mutations

Yo Jun Choi

Department of Medical Science
The Graduate School, Yonsei University

(Directed by Professor Heon Yung Gee)

I. INTRODUCTION

Primary cilium is a solitary and sensory organelle that responds to chemical and mechanical stimuli in the environment and transmits the external signal to the cell's interior in order to regulate development and tissue homeostasis[1]. In the kidney, primary cilia sense urine flow and are essential for the maintenance of epithelial architecture. Primary cilia consist of a microtubule based axoneme, assembled from a basal body, transition zone[2]. Defects in primary cilia cause a group of heterogenous diseases called ciliopathy, including nephronophthisis, Bardet-Biedl syndrome, Joubert syndrome, Senior-Loken syndrome[3,4].

Nephronophthisis (NPHP) is genetic disorder of the kidneys which affects children. The disease is inherited in an autosomal recessive manner. NPHP is characterized by tubular basement membrane (TBM) disintegration with irregular thickening, and interstitial round cell infiltration with fibrosis, and later on, the formation of cysts occurring mainly at the cortico- medullary junction[5]. Some individuals suffer from NPHP also present with extrarenal symptoms, including retinitis pigmentosa, intellectual disability, cerebellar ataxia, bone anomalies, or liver fibrosis. These

syndromes called NPHP-related ciliopathies (NPHP-RCs), are degenerative recessive diseases in the kidney, liver, retina, and central nervous system[5].

More than 90 genes have been reported as a monogenic recessive cause of NPHP-RC, which accounts for 50~60% of NPHP-RC cases according to the composition of the examined cohort[6]. Therefore, many NPHP-RC cases is unsolved. We performed homozygosity mapping and whole exome sequencing for or >100 affected individuals born from consanguineous parents or siblings of index individuals who were affected by NPHP-RC. In an analysis combined with high-throughput exon sequencing in a cohort of 800 individuals with NPHP-RC, we found *ADAMTS9* as a novel renal ciliopathy gene in four individuals with early-onset ESRD and NPHP with various extrarenal symptoms including short stature, deafness, developmental delay. We aim to investigate and characterize the pathogenicity of ADAMTS9 mutations (p.T65R, p.Q1525Hfs*60, p.C1024* and p.S636F) identified in individuals with NPHP-RC.

A disintegrin and metalloproteinase with thrombospondin motifs (ADAMTS) family is known as multidomain extracellular metalloproteinase enzymes with 19 members that regulate extracellular matrix (ECM) composition and facilitate cell migration by removing barriers such as proteoglycan and collagen[7-9]. Extracellularly, ADAMTS9 is known to cleave versican in the ECM and plays an essential role in promoting vascular smooth muscle cell differentiation through proteolysis of versican during umbilical cord vascular development in mice[10]. In addition to its canonical role as a ECM metalloproteinase, ADAMTS9 is located near the basal body of the primary cilia intracellularly and involved in ciliogenesis[11,12]. *adamts*9-null mice are embryonic lethal[13], but *Adamts9*$^{+/-}$ heterozygous mice result in abnormality in heart formation[14]. Zebrafish, in which adamts9 is knocked down, exhibited abnormal body axis, kidney cyst, and hydrocephalus[11].

In addition, kidney organoids derived from iPSCs have the potential to model how kidney development, disease, and injury in vitro. it is known that the ECM can affect primary cilia formation and function and renal cystogenesis is controlled by stromal composition[15]. To mimic the in vivo physical and biochemical environment, we generate ADAMTS9 knock-out in Induced Pluripotent Stem cells using CRISPR/Cas9

and induce differentiation of the *ADAMTS9* knock out iPSC into kidney organoid. We aim to elucidate genetic factors in patients with nephronophthisis caused by ADAMTS9 mutations and identify the intracellular function of ADAMTS9 near the basal body of primary cilia.

II. MATERIALS AND METHODS

1. Whole-exome sequencing

Whole-exome sequencing (WES) was performed using Agilent SureSelect human exome capture arrays with next-generation sequencing (NGS) on the IlluminaTM sequencing platform. Sequence reads were mapped against the human reference genome (NCBI build 37/hg19) using CLC Genomics Workbench (version 9.0.1) software (Qiagen Inc., Germantown, MD, USA). Variant calling and filtering were performed as previously described[16].

2. Plasmid Construction and Site-Directed Mutagenesis

The cDNA for human ADAMTS9 was purchased from OriGene Technologies and was subcloned into the pENTR-D-TOPO vector (Invitrogen, Waltham, MA, USA). Expression vectors were created with LR clonase (Invitrogen, Waltham, MA, USA) according to the manufacturer's instructions. Clones reflecting the ADAMTS9 mutations that were identified in individuals with NPHP-RC were introduced into the cDNA constructs in the pENTR-D-TOPO vector with a QuikChange II XL site-directed mutagenesis kit (Agilent Technologies, Santa Clara, CA, USA).

3. Cell Culture and Transfection

Mouse inner medullary collecting duct-3 (IMCD3, CRL-2123) and hTERT retinal pigment epithelial-1 (RPE1, CRL-4000) cells were obtained from the American Type Culture Collection (ATCC, Manassas, VA, USA) and cultured in DMEM/F12 with 10% fetal bovine serum (FBS) and penicillin (50 IU/mL) and streptomycin (50 mg/mL). ADAMTS9-specific and control-scrambled short interfering RNAs (siRNAs) were purchased from Dharmacon (Lafayette, CO, USA). The siRNAs were transfected into RPE1 cells via MISSION siRNA transfection reagent (Sigma-Aldrich, St. Louis, MO, USA). So that Adamts9 knockout (KO) could be achieved, IMCD3 cells were transduced with lentivirus containing lentiCRISPR v2 (Addgene plasmid #52961) (Watertown, MA, USA), and transformants were selected and maintained with 4

mg/mL puromycin. The target sequences of siRNAs and single guide RNAs (sgRNAs) used in this study are shown in Table 1-3. Human embryonic kidney 293 (HEK293) cells were cultured in DMEM supplemented with 10% FBS and penicillin (50 IU/ml) and streptomycin (50 mg/ml) (Invitrogen, Waltham, MA, USA). The cells were transfected with plasmids via Lipofectamine and PLUS reagent, or Lipofectamine 2000 (Invitrogen, Waltham, MA, USA), according to the manufacturer's instructions.

4. Immunoblotting and Immunofluorescence

Cell cultures were washed once with PBS and fixed in 4% paraformaldehyde for 15 min at room temperature (RT). Fixed cells were washed three times in PBS and incubated in blocking buffer (0.3% Triton X-100 and 5% normal Goat serum) for 1 hr at RT. The cells were then incubated with primary antibody overnight at 4°C.

Anti-ADAMTS9 (Novus, NBP1-82916, Centennial, CO, USA), anti-b-actin (Abcam, ab6276, Cambridge, MA, USA), anti-g-tubulin (Abcam, ab11316, Cambridge, MA, USA), anti-acetylated-a-tubulin (Abcam, ab24610, Cambridge, MA, USA), anti-Myc (Santa Cruz Biotechnology, sc-40 and sc-789, Santa Cruz, CA, USA), anti-V5 (Invitrogen, R-960-25, Waltham, MA, USA), anti-acetylated-a-tubulin (Sigma-Aldrich, T7451, St. Louis, MO, USA), anti-GLI1 (Cell Signaling Technology, #2534, Danvers, MA, USA), and anti-GLI3 (R&D Systems, AF3690, Minneapolis, MN, USA) antibodies were obtained from commercial sources. Alexa 488-, Alexa-594-, and Alexa-647-conjugated secondary antibodies and DAPI (40,6-diamidino-2-phenylindole dihydrochloride) were obtained from Invitrogen (Waltham, MA, USA). HRP-labeled secondary antibodies were purchased from Santa Cruz Biotechnology (Santa Cruz, CA, USA). Confocal images were obtained with a Carl Zeiss LSM780 microscope (Carl Zeiss, Berlin, Germany) or Leica SP5X system (Leica Biosystems, Nussloch, Germany) with an DM6000 upright compound microscope. Image processing and analysis were performed with the ZEN software (Carl Zeiss, Berlin, Germany) or Leica AF suite (Leica Biosystems, Nussloch, Germany). For immunofluorescence, IMCD3 or RPE1 cells were seeded at a low density and grown

to 80% confluence. For ciliation analysis, RPE1 cells were grown to confluence and then starved of serum for 48 hr.

5. Scanning Electron Microscopy

The cells were fixed with 2% glutaraldehyde-paraformaldehyde in 0.1Mphosphate buffer (pH 7.4) for 6 hr and washed two times for 30 min each with 0.1Mphosphate buffer. They were post-fixed for 1.5 hr with 1% OsO4 that was dissolved in 0.1M phosphate buffer. Then, cells were dehydrated in an ascending, gradual series (50%–100%) of ethanol, and samples were treated with isoamyl acetate and subjected to a critical-point dryer (Leica EM CPD300) (Leica Biosystems, Nussloch, Germany). They were coated with platinum (5 nm) by an ion coater (Leica EM ACE600) (Leica Biosystems, Nussloch, Germany) and examined with a scanning electron microscope (Carl Zeiss FE-SEM) (Carl Zeiss, Berlin, Germany) at 7 kV.

6. Real-Time PCR

RNA samples were isolated from RPE1 cells with RiboEx (GeneAll Biotechnology, Seoul, Korea) and reverse-transcribed with an iScript cDNA Synthesis Kit (Bio-Rad, Hercules, CA, USA). Samples were assayed with SYBR Green ready master mix and ROX reference dye (Takara Bio Inc., Shiga, Japan); primers are listed in Table 4. Real-time PCR was performed with the StepOnePlus Real-Time PCR System (Applied Biosystems, Waltham, MA, USA). The relative RNA expression levels were calculated via a comparative threshold cycle (Ct) method that used glyceraldehyde 3-phosphate dehydrogenase (GAPDH) as a control.

7. Spheroid Assay

Spheroid assays were performed as previously described[17]. Control and Adamts9 KO IMCD3 cells were trypsinized, and resuspended cells were then mixed 1:1 with growth-factor-reduced Geltrx (GIBCO) and seeded on a Nunc Lab-Tek II chambered coverglass (Thermo Fisher Scientific, Waltham, MA USA). After 72 hr, the cells were stained and imaged with a Zeiss LSM700 confocal microscope (Carl Zeiss, Berlin,

Germany), which identified spheroids with visible cleared lumens. For rescue experiments, IMCD3 cells were transfected with human ADAMTS9 cDNA constructs and, after 24 hr, were trypsinized. In each spheroid, nuclei were counted.

8. Rearing Zebrafish Embryos and Microinjecting Morpholinos and mRNA

Approval for zebrafish (Danio rerio) research was obtained from the University Committee on the Use and Care of Animals (UCUCA) of the Boston Children's Hospital and Yonsei University College of Medicine. Wild-type zebrafish embryos were obtained from natural spawnings of AB-line fish and raised at 28.5℃. A standard control and adamts9 morpholinos (MOs) were designed and purchased from Gene Tools. Fertilized eggs were microinjected at the 1- to 2-cell stage with 0.2 mM MOs diluted in 200 mM KCl, 0.1% phenol red (Sigma-Aldrich, St. Louis, MO, USA), and 10 mM HEPES. The scoring of cyst formation and zebrafish embryo imaging were conducted on mixed male and female embryos 48 hr after fertilization under a Leica MZ16 stereo microscope (Leica Biosystems, Nussloch, Germany). For histological analysis, zebrafish embryos were fixed with 4% paraformaldehyde overnight at 4℃; dehydrated with an ethanol series of 25%, 50%, 75%, and 95% ethanol; and equilibrated with JB-4 solution (Polysciences, Warrington, PA, USA) overnight at 4℃. The zebrafish embryos were then embedded in JB-4 resin and sectioned with a Leica R2265 microtome (Leica Biosystems, Nussloch, Germany). The 6 mm sections were then stained with methylene blue.

9. Maintenance of hiPSCs

IMR90, human iPSCs (hiPSC derived from healthy fibroblasts; passage 16) were maintained in mTeSR1 (STEMCELL, #85850, Vancouver, Canada) in 6-well tissue culture plates (Falcon, #353046, New York, NY, USA) coated with iMatrix-511 (Nippi, Yokohama, Japan) in a 37°C incubator with 5% CO_2. hiPSCs were passaged using Dissociation Solution for ReLeSR (STEMCELL, #05872, Vancouver, Canada) at a 1:5 split ratio every 4~5 days according to the manufacturer's protocol. IMR90 was purchased from Applied StemCell (Milpitas, CA, USA). The ADAMTS9 knockout

hiPSC line was generated from the IMR90 hiPSC line and maintained as described above.

10. Differentiation of hiPSCs

hiPSCs grown on iMatrix-511 were washed once with PBS (Life Technologies, #10010-049) (Thermo Fisher Scientific, Waltham, MA USA) and dissociated into single cells with Accutase (STEMCELL Technologies, #07920, Vancouver, Canada). Cells were then plated at a density of 1×10^4cells onto 96-well low-cell-binding V bottom plates (S-BIO, MS-9096VZ, Hudson, NH, USA) in the presence of 20 ng/ml human bFGF, 10 mM Y27632 and 1 ng/ml human Activin A (Day 0). After 24 hr (Day 1), the spheres were transferred to U-bottom 96-well low cell-binding plates containing mesoderm-inducing medium with 10 mM CHIR and 10 mM Y27632. Subsequently, half of the culture medium was refreshed with new medium every other day (on days 3 and 5). On day 7, the medium was changed to medium containing 10 ng/ml human Activin A, 3 ng/ml human Bmp4, 3 mM CHIR, 0.1 mM Retinoic acid, and 10 mM Y27632. On day 10, the medium was changed to medium containing 1 mM CHIR, 5 ng/ml human Fgf9, and 10 mM Y27632[18].

11. 3D kidney organoid formation

At day 13, induced spheres were analyzed by flow cytometry to measure the percentages of ITGA8+/PDGFR- nephron progenitors in the spheres. The percentages were more than 50%.The remaining spheres were cultured with 3 mM CHIR in Trans well inserts (#3428; Costar, Washington, D.C., USA) with the medium containing Knock Out Serum Replacement (#10828010; Thermo Fisher Scientific, Waltham, MA USA). After that, the organoids were cultured in the medium with no additional factors for 14–30 days[18].

12. Flow cytometric analysis

Induced cell aggregates from hiPSCs were dissociated and blocked with normal mouse serum for 10 min on ice. Cell surface marker staining was carried out in 1 x

HBSS containing 1% BSA and 0.035% NaHCO3 for 15 min on ice. Stained cells were analyzed using a FACS Verse I (BD Biosciences, San Jose, CA, USA). For cell sorting, stained cells were sorted using a FACS SORP Aria (BD Biosciences, San Jose, CA, USA).

13. Statistical Analysis

The results are presented as the means 5 standard deviation for the indicated number of experiments. Statistical analysis of continuous data was performed with two-tailed Student's t tests. $p < 0.05$ was considered statistically significant.

Table 1. Target sequences of sgRNAs used in this study

Mouse ADAMTS9	
sgRNA#1	TTAGGAACCCAGCGCACACT
sgRNA#2	CTTAGGAACCCAGCGCACAC
sgRNA#3	GTCTCCTTCCAAGTGTGCGC

Table 2. Target sequences of sgRNAs used in this study

Human ADAMTS9	
sgRNA#1	GAGCGAATACGAAATCGTGT
sgRNA#2	CTTCAAAAGAACGCGACGGA
sgRNA#3	CCAATGCCGGATTTATCGCT

Table 3. Target sequences of siRNAs used in this study

Human ADAMTS9	
siRNA#5	CGACAAAUGUGAUACCUUA
siRNA#7	GCCAAUGUCGGAAGGAUUA
siRNA#8	CGAGGCAAGUGAAAUUAUU

Table 4. Sonic Hedgehog signaling *RT PCR* primers

Gene related to Sonic Hedgehog signaling	
SHH Forward	GAT GTC TGC TGC TAG TCC TCG
SHH Reverse	CAC CTC TGA GTC ATC AGC CTG
Smo Forward	GTT CTC CAT CAA GAG CAA CCA
Smo Reverse	CGA TTC TTG ATC TCA CAG TCA GG
GLi1 Forward	GGG ATG ATC CCA CAT CCT CAG TC
GLi1 Reverse	CTG GAG CAG CCC CCC CAG T
GLi2 Forward	TGG CCG CTT CAG ATG ACA GAT GTT G
GLi2 Reverse	CGT TAG CCG AAT GTC AGC CGT GAA G
GAPDH Forward	GGCCGAGGGCCCACTA
GAPDH Reverse	TGTTGAAGTC ACAGGAGACA ACCT

III. RESULTS

1. ADAMTS9 Mutations Cause NPHP-RC

To identify additional genes mutated in NPHP-RC, we performed whole exome sequencing in >100 consanguineous individuals or siblings of index individuals who were also affected with NPHP-RC. A child of European origin (F1279-21) was 5 years of age and had end-stage renal disease (ESRD) from NPHP and phenotypes characteristic of Joubert syndrome (MIM: 213300); such phenotypes included corpus callosum hypoplasia and aplasia of the vermis (Figures 1A-B and Table 5). In addition, individual F1279-21 presented with proteinuria, deafness, atrial septal defects, coloboma, and short stature (Table 5). WES detected a homozygous truncating mutation (c.4575_4576del [p.Gln1525Hisfs*60]) in ADAMTS9 [MIM: 605421] [GenBank: NM_182920.1]) (Figures 1C, 1I and Table 5). To discover additional mutations in ADAMTS9, we performed high-throughput exon sequencing in a worldwide cohort of 800 additional families affected by NPHP-RC[19]. We detected a homozygous missense variant (c.194C>G [p.Thr65Arg]) in ADAMTS9 in an Arabic child (A5048-21) from consanguineous parents (Table 5 and Figure 1D). We additionally performed WES of individual A5048-21 and excluded mutations in genes previously linked to NPHP-RC. The variant (c.194C>G [p.Thr65Arg]) in ADAMTS9 is reported as a SNP in the dbSNP database; however, its minor-allele frequency is 0.0002, and it does not appear in the homozygous state in the gnomAD database (Figures 1F, 1I and Table 5). In addition, multiple tools have predicted it to be deleterious for protein function, and it alters an amino-acid residue that is evolutionarily conserved from humans down to *Caenorhabditis elegans* (Table 5 and Figure 1I). Individual A5048-21 showed increased echogenicity on ultrasound (Figure 1E) and had proteinuria, deafness, hepatosplenomegaly, anemia, thrombocytopenia, short stature, and osteopenia and had had ESRD due to NPHP since infancy (Table 5). Another index patient was 8-year 7-month-old Caucasian female had prenatal history of abnormality in the ultrasounds, including hydrocephaly. The patient revealed bilateral abnormal echogenic kidneys with decreased corticomedullary differentiation on renal ultrasound, a single simple-

appearing cyst on the right and bifid right upper renal collecting system. She had multiple congenital anomalies including coloboma, absence or agenesis of corpus callosum, bicornate uterus, anorectal anomaly, and a tied tongue (Table 5 and Figure 1G). There is an older sister who also had overlapping congenital anomalies with bilateral iris and retinal coloboma, agenesis of corpus callosum, bicornate uterus and mild anorectal problem. To identify the possible genetic cause, WES was performed on the index patient. Biallelic mutations at the sites c.1907C>T (genome position, chr : 64601114) and c.3072T>A (genome position, chr : 64601114) of the ADAMTS9 gene (NM_182920.1) were detected, resulting in a missense (p.Ser636Phe) and a nonsense (p.Cys1024*) variant, respectively. Segregation analysis using Sanger sequencing confirmed that her father was heterozygous for c.1907C>T, her mother was heterozygous for c.3072T>A, and the older sister had both mutation, indicating that the identified mutations were segregated with the affected status in the family (Figures 1G, 1H, 1I). In silico prediction indicated that this nucleotide position of ADAMTS9 is highly conserved during evolution and the serine at the 636th residue is identical among 6 vertebrate species, suggesting that this conserved residue might be essential for ADAMTS9 function (Figure 1I). The c.1907C>T in ADAMTS9 was novel missense mutation and was not reported in the HGMD1, ClinVar2 and gnomAD database. In addition, multiple tools have predicted it to be deleterious for protein function. The missense mutation was predicted to be deleterious by SIFT with score 0, disease causing by Mutation Taster with score 1.00, and damaging by CADD with score 29.4. The c.3072T>A in ADAMTS9 was novel nonsense mutation and was not reported in the HGMD1, ClinVar2 and gnomAD database. This mutation was predicted to be damaging by CADD with score 35.0 (Table 5).

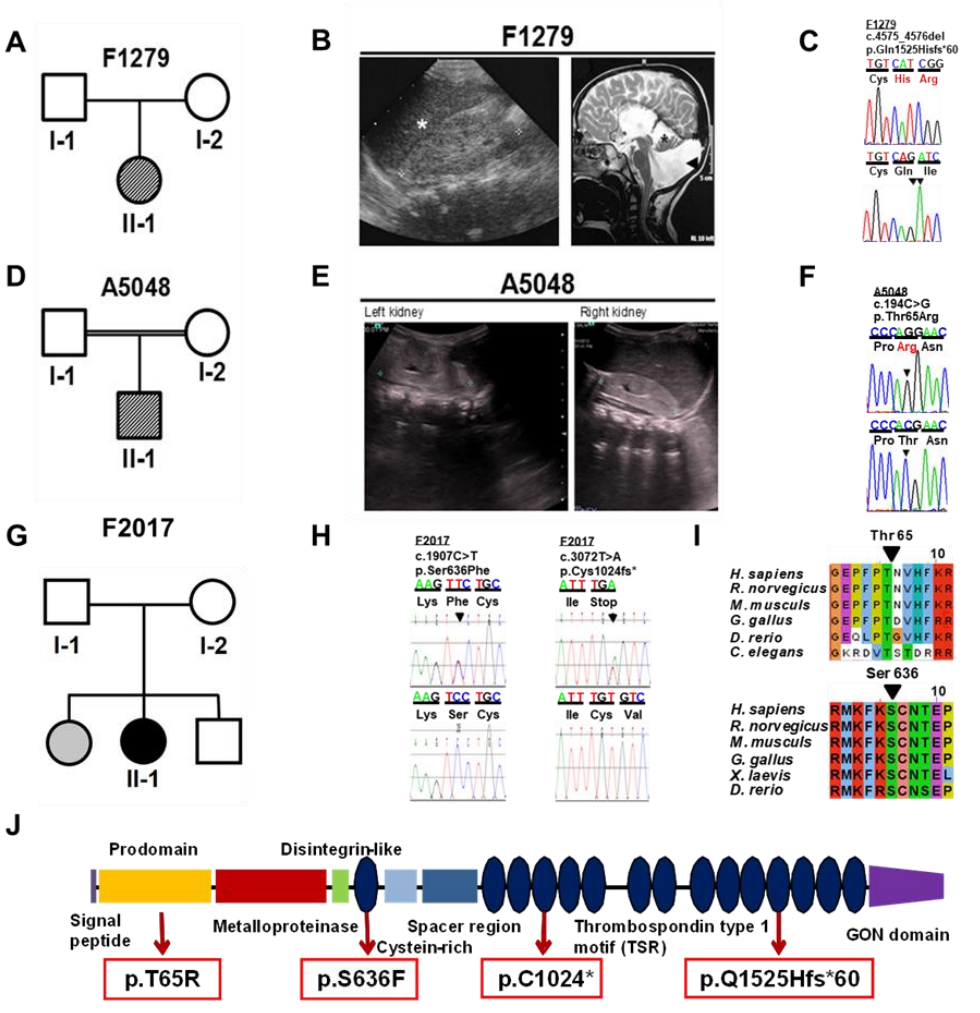

Figure 1. Whole-exome sequencing detection of ADAMTS9 mutations in individuals with NPHP-RC. **(A)** A child of European origin was 5 years of age and had end-stage renal disease from NPHP and phenotypes characteristic of Joubert syndrome. WES detected a homozygous truncating mutation in ADAMTS9. Ultrasound (US) of right kidney of F1279-21 shows increased echogenicity (*). **(B)** Brain MRI of F1279-21. Sagittal image shows cystic dilation of the fourth ventricle (arrowhead), cephalad rotation of the vermian remnant (*), and elevation of the torcular herophili and sinus rectus (#) **(D)** A child of consanguineous parents in Arabic, the

representative symptom is also NPHP. **(E)** US of the right kidney of A5048-21 shows increased echogenicity compared to that of liver (*). **(C),(F),(H)** Sanger sequencing traces show altered nucleotides (arrowheads). **(G)** A 8-year-old Caucasian female has end-stage renal disease with significant medical history for multiple congenital anomalies, including a right duplicated kidney, bicornuate uterus, bilateral optic and retinal coloboma, absence or agenesis of corpus callosum. **(I)** Protein alignment analysis shows high evolutionary conservation for serine residue at position 636 and Threonine residue at position 65 of the ADAMTS9 protein across multiple species. **(J)** ADAMTS9 has a signal peptide, prodomain, metalloproteinase domain, disintegrin-like domain, thrombospondin type 1 motifs, and GON-1 domain. The locations of amino acid residues affected by mutations in ADAMTS9 detected in individuals with NPHP-RC are indicated. p.S636F, p.C1024*, p.T65R and p.Q1525Hfs*60 are mutations we found.

Table 5. Phenotypes of individuals with recessive ADAMTS9 mutations

Family -Individual	Nucleotide change	Amino acid change	Exon (Zygosity, Segregation)	Amino acid conser-vation to species	gnomAD allele frequencies	MT	CADD	SIFT	Gen-der	Ethnic origin	Renal manifestation	Renal biopsy	Extrarenal Manifestations
F1279 -21	c.4575_4576del	p.Gln1525Hisfs*60	Exon 30 (HOM)	N/A	ND	N/A	N/A	N/A	F	European	increased echogenicity, medullary cysts, proteinuria ESRD at 5 yr	ND	cortical deafness ASD growth retardation coloboma aplasia of vermis, corpus callosum hypoplasia
A5048 -21	c.194C>G	p.Thr65Arg	Exon 2 (HOM)	C. elegans	0.0002409 (1 homozygote)	DC (1.00)	23.5	Del(1.00)	M	Arabic	NPHP, nonselective proteinuria, ESRD since infancy	microcystic dilatation of tubules immature glomeruli (at 2 yr)	sensorineural deafness hepatosplenomegaly short stature anemia, thrombocytopenia osteopenia, rickets
-F2017	c.1907C>T c.3072T>A	p.S636F p.C1024*	Exon 13 (het, F) Exon 21 (het,M)	*D.rerio* N/A	ND ND	DC (1.00) N/A	29.4 35	Del(0) N/A	F	Caucasian	nephrotic range proteinuria, bilateral abnormal echogenicity, bifid right upper renal collecting system, bilateral single cyst ESRD at 5 yr.	Irregularly increased mesangial matrix with moth eaten appearance global sclerosis with tubular atrophy and interstitial fibrosis glomerular capillary loops with membrane duplication cellular interposition, subendothelial and intramembranous deposit C3 glomerulonephritis	hypertension hydrocephaly bicornate uterus anorectal abnormalities bilateral retinal coloboma absence or agenesis of corpus callosum short stature tied tongue
-Older sister of F2017									F				hypoplastic left heart syndrome bilateral iris, retinal coloboma agenesis of corpus callosum bicornate uterus

Abbreviations are as follows: ASD, atrial septal defect; CADD, Combined Annotation Dependent Depletion; C.e, C. elegans; D.r, Danio rerio; DC, disease causing; Del, deleterious; ESRD, end-stage renal disease; F, female; gnomAD, Genome Aggregation Database; het, heterozygous; HOM, homozygous; M, male; MT, mutation taster; NA, not applicable; ND, no data; NPHP, nephronophthisis; SIFT, sorting Intolerant From Tolerant; yr, years. ADAMTS9 cDNA mutations are numbered according to human cDNA reference sequence NM_182920.1.

2. ADAMTS9 Localizes Near Basal Bodies of Primary Cilia

Since NPHP-RC protein is localized to primary cilia, centrosomes, mitotic spindles, and abscission structures at various stages in the cell cycle[20], we first investigated the localization of ADAMTS9 in cell lines with primary cilia. Surprisingly, ADAMTS9 was detected near the basal bodies of primary cilia during interphase in human dermal fibroblasts, RPE1 cells, mouse embryonic fibroblasts, and IMCD3 cells (Figure 2A). In addition, ADAMTS9 was also observed in vesicular structures in the cytoplasm of human fibroblasts (Figure 2A, arrows). To examine whether exogenous ADAMTS9 can be targeted to basal bodies, we transfected RPE1 cells with C-terminal Myc-tagged ADAMTS9 (ADAMTS9-Myc). When overexpressed, wild-type ADAMTS9, like endogenous ADAMTS9, localized near the base of primary cilia (Figure 2B), whereas neither p.Thr65Arg nor p.Gln1525Hisfs*60 mutant proteins were observed near the basal body (Figures 2C, 2D and 2E). The other mutations (p.Cys1024* and p.Ser636Phe) were also transfected with C-terminal V5-tagged wild type and mutant ADAMTS9 plasmids. Wild-type ADAMTS9 localized near the base of primary cilia as expected, whereas p.Cys1024* mutant protein was not located near the basal body of primary cilia (Figure 2H). In the case of p.Ser636Phe ADAMTS9, it was observed in some cells, but not in most cells (Figures 2G-G'). Statistical analysis showed that p.Ser636Phe mutant protein was not present at the base of in 70% of all transfected cells with existing primary cilia (Figure 2I). p.Gln1525Hisfs*60 and p.Cys1024*, a frameshift mutation that resulted in a truncated protein with loss of both several thrombospondin motifs and the GON domain, completely lose its function. Whereas p.Ser636Phe, missense mutation in disintegrin-like domain of ADAMTS9, the ability to locate near the base of the primary cilia reduced, suggesting that this mutation is functionally hypomorph (Figure 1I).

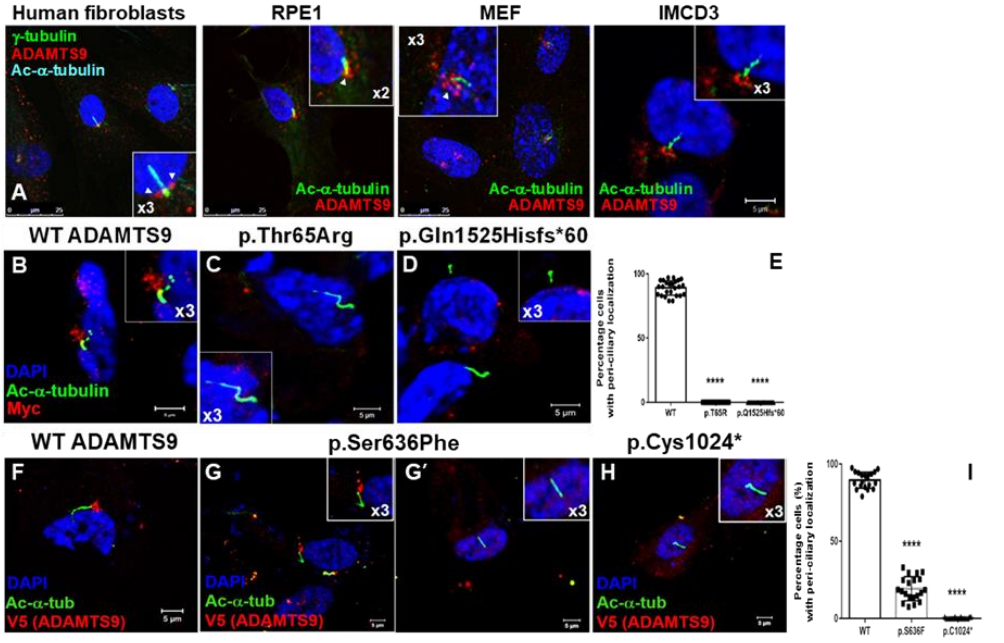

Figure 2. ADAMTS9 localizes near the basal body of primary cilia. (A) Localization of ADAMTS9 in ciliated human dermal fibroblasts, retinal pigment epithelium-1 (RPE1) cells, mouse embryonic fibroblasts (MEFs), and inner medullary collecting duct-3 (IMCD3) cells. **(B-D),(F-H)** Localization of exogenous ADAMTS9 in RPE1 cells. RPE1 cells were transfected with C-terminal Myc-or V5-tagged wild type (WT) and mutant ADAMTS9 cDNA constructs, serum-starved for 48 hr, and then stained with Ac-a-tubulin and Myc. **(E),(I)** Percentage of cells with peri-ciliary localization **(B-D and F-H)**. Experiments were repeated more than three times independently, and more than 100 cells were counted in each experiment.

3. Wild type and mutant ADAMTS9 proteins do not affect expression and secretion

In order to reveal the pathogenicity of ADAMTS9 mutations, we examined in the effects of variants on expression and secretion at the protein level. The expression levels of wild-type and both mutant ADAMTS9 in cell lysates were comparable, which suggesting that these mutations does not affect expression or intracellular stability. When we examined ADAMTS9 proteins in the culture media, both mutant proteins were not different from wild-type ADAMTS9, indicating that these mutations does not cause defects in the secretion of ADAMTS9 into the extracellular space (Figures 3A-B). It was revealed that ADAMTS9 protein is secreted to the extracellular space, and then re-localized near the basal bodies of primary cilia[12]. As the expression and secretion of mutant ADMATS9 proteins were normal, we investigated whether endocytosis of ADAMTS9 after secretion allowed its localization near the basal body. To solve this question, we transfected RPE1 cells with the ADAMTS9-Myc construct and treated them with an endocytosis inhibitor, either Dynasore or Pitstop 2. The ciliary localization of ADAMTS9 was not observed after treatment with either inhibitor (Figures 4A–4E). In addition, overexpression of wild-type dynamin did not affect the localization of ADAMTS9 near the basal body (Figure 4D), whereas this localization was inhibited by overexpression of dominant-negative dynamin (K44A, Figure 4E). These data indicated that endocytosis is required for the localization of ADAMTS9 near the basal bodies.

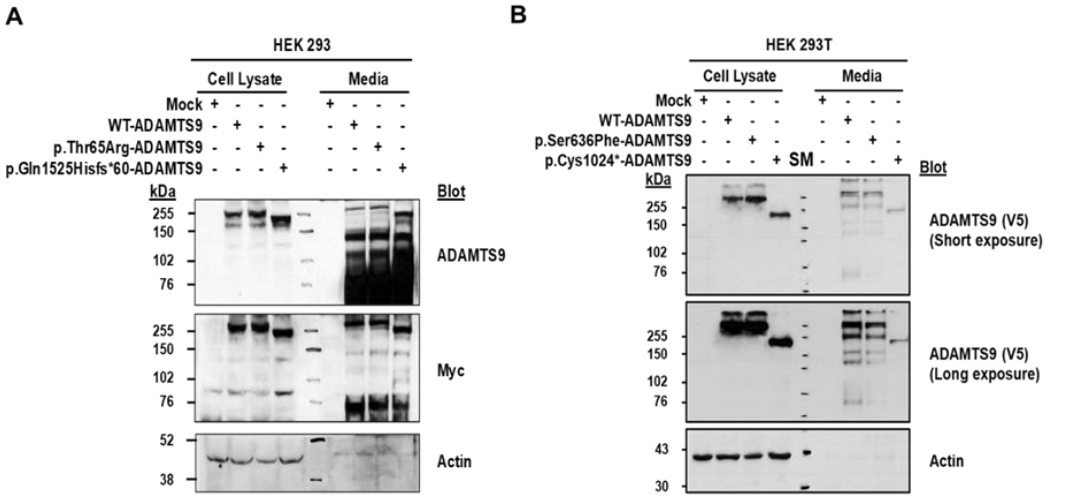

Figure 3. Expression and secretion of wild type and mutant ADAMTS9 proteins. **(A-B)** Human embryonic kidney 293 (HEK 293) cells were transfected with C-terminal Myc-**(A)**, V5-**(B)** tagged wild type (WT) or mutant ADAMTS9 plasmids using Lipofectamine PLUS reagent according to the manufacturer's instructions. After 24 hr, medium was changed to serum-free medium. After 60 hr, cells were harvested and lysed. Serum-free medium were collected separately and concentrated using Amicon Ultra-4 (Milipore). The protein samples were separated by SDS polyacrylamide gel electrophoresis. The separated proteins were transferred to a nitrocellulose membrane and blotted with the indicated primary antibodies.

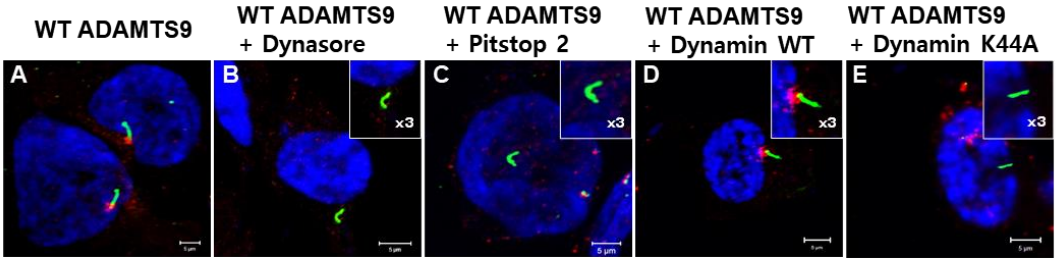

Figure 4. Effect of endocytosis inhibition on the localization of exogenous WT ADAMTS9. (A) Localization of ADAMTS9 in ciliated human retinal pigment epithelium-1 (RPE1) cells. Note that treatment with the endocytosis inhibitor Dynasore **(B)** or Pitstop 2 **(C)**, or overexpression of dominant-negative Dynamin (K44A) **(E)** prevented the localization of WT ADAMTS9 near the basal body **(D)**.

4. Loss of ADAMTS9 Results in Defects in Primary Cilia

Since ADAMTS9 mutations appear to cause NPHP-RC and because ADAMTS9 localizes near the basal bodies of primary cilia, we investigated the effects of ADAMTS9 on ciliogenesis. We first generated IMCD3 cells in which Adamts9 was knocked out via the CRISPR/ Cas9 system. Two Adamts9 knockout (KO) cells, KO#1 (c.275_279del [p.Trp92Serfs*2]) and KO#2 (c.269_270del [p.Val90Alafs*5]), were confirmed by Sanger sequencing and immunoblotting. Upon serum starvation, Adamts9 KO cells had shorter primary cilia than control IMCD3 cells (Figures 5A and 5C). Scanning electron microscopy also confirmed that knockout of Adamts9 resulted in shortened primary cilia (Figure 5B). *Adamts9* KO IMCD3 cells showed a statistically significant reduction in the percentage of ciliated cells compared to control IMCD3 cells (Figure 5D). Because hedgehog (hh) signaling is mediated through primary cilia[21] and sonic hh (Shh) signaling is defective in Adamts9Gt/Gt vascular smooth muscle cells[22], we examined Shh signaling in RPE1 cells. The translocation of smoothened (SMO) into primary cilia upon Shh pathway activation was investigated through the use of RPE1 cells that stably expressed GFP-tagged SMO. SMO-GFP was observed at the base of primary cilia; however, upon stimulation by SAG (a chlorobenzothiophene-containing compound that acts as a SMO agonist), SMO-GFP signals became stronger and were observed along ciliary axoneme. When ADAMTS9 was knocked down by siRNA, the translocation of SMO-GFP into shortened primary cilia was not observed upon SAG treatment. (Figure 5F) The addition of 100 nM SAG to RPE1 cells for 24 hr resulted in increased mRNA amounts of SMO, GLI1, and GLI2 in comparison to baseline amounts without SAG stimulation. In contrast, ADAMTS9 knockdown with two different siRNAs reduced the upregulation of Shh target genes, indicating defects in the primary cilia. After ADAMTS9 knockdown by siRNA transfection, we observed decreased GLI1, consistent with the real-time PCR data (Figure 5E). To further confirm a defect in Shh signaling, we measured the levels of the full-length GLI3 (GLI3FL) and repressor (GLI3R) forms. When the Shh ligand is not present, GLI3FL is cleaved into GLI3R, and this cleavage is inhibited by activation of Shh pathways[23]. In control RPE1 cells, SAG treatment reduced the levels of both GLI3FL and GLI3R. However, in cells

transfected with ADAMTS9 siRNA, neither the amount ofGLI3FL nor that of GLI3R decreased upon SAG treatment (Figure 5G).

To elucidate the role of ADAMTS9 in the pathogenesis of NPHP-RC, we examined the effects of Adamts9 KO by using a 3D spheroid model, a well-established model for recapitulating polarity defects seen in NPHP-RC[17]. Control IMCD3 cells developed spheroids with a clear lumen surrounded by a monolayer of cells, apical cilia, and clear apicobasal polarity (Figure 6A). By contrast, Adamts9 KO IMCD3 cells formed defective spheroids characterized by mislocalized b-catenin at the basolateral membrane and an irregular lumen surrounded by multiple layers of cells (Figures 6B and 6C). This defect could be partially rescued by concurrent transfection with wild-type human ADAMTS9 (Figure 6D), but not with either ADAMTS9 mutant (Figures 6E and 6F). Figure 6G shows quantification of these results. Taken together, these findings indicated that the identified mutations induced the loss of the ciliary function of ADAMTS9.

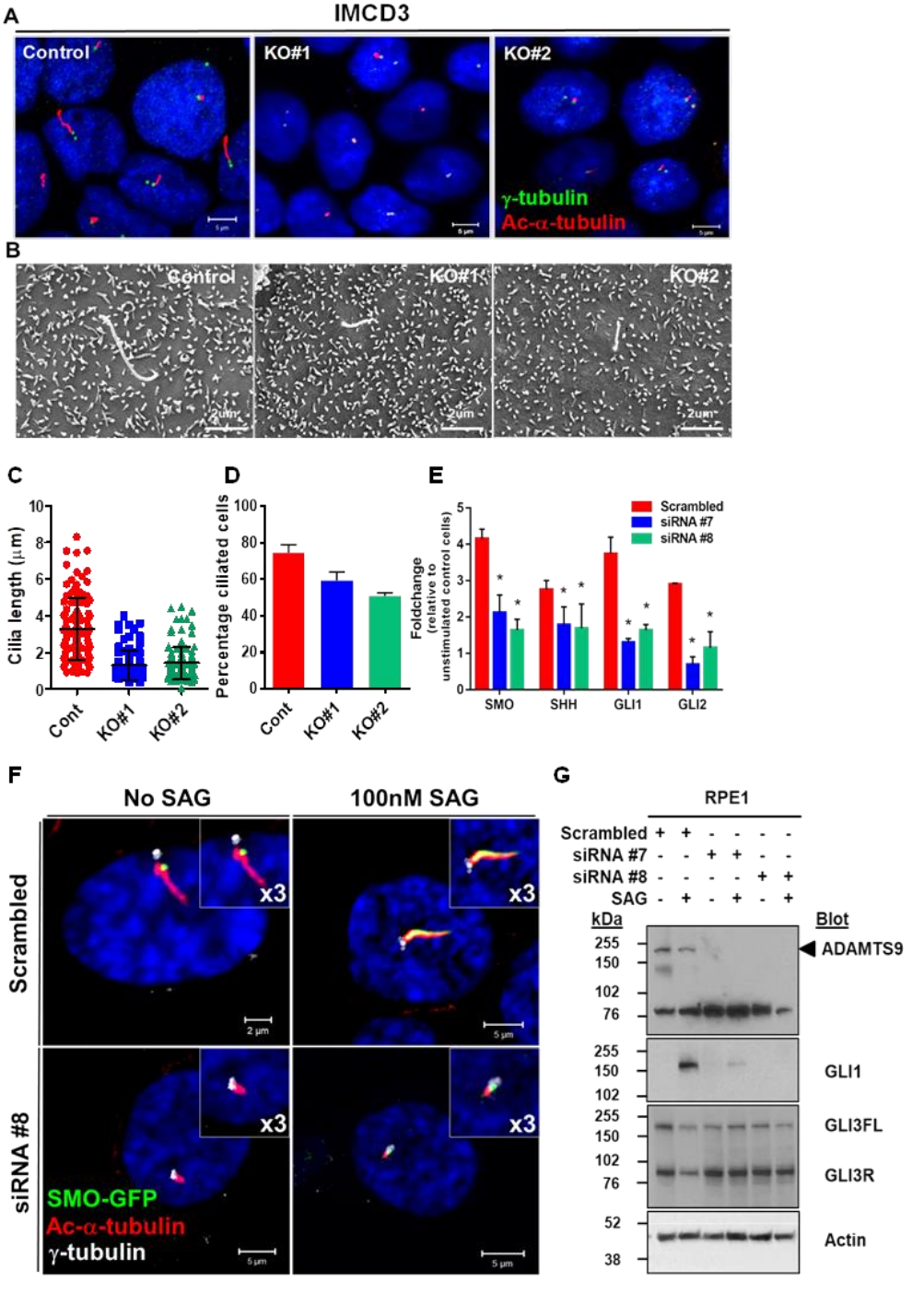

Figure 5. Loss of ADAMTS9 causes defects in primary cilia. (A) Effect of Adamts9 knockout (KO) using CRISPR/Cas9 system on primary cilia in IMCD3 cells. The length of the primary cilia of IMCD3 cells was shortened by Adamts9 KO. Cells were serum-starved for 48 hr and then stained with acetylated-a-tubulin (Ac-a-tubulin) and γ-tubulin. **(B)** Scanning electron microscopy images of primary cilia of control and Adamts9 KO cells. **(C)** Cilium length was measured based on Ac-a-tubulin staining in >100 cells per condition. *P < 0.05, t-test. **(D)** Percentage of ciliated cells. Experiments were repeated more than three times independently, and more than 100 cells were counted in each experiment. Data represent mean + standard deviation (SD). *P < 0.05, t-test. **(E)** Translocation of SMO into primary cilia is defective upon ADAMTS9 knockdown by siRNA. **(F)** Effects of ADAMTS9 knockdown on sonic hedgehog (Shh) signaling in RPE1 cells. Upon stimulation by 100 nM smoothened (SMO) agonist (SAG), Shh target genes were upregulated in control cells but not in cells treated with siRNAs. Data represent mean + SD of four independent. experiments. *P < 0.05, t-test. **(G)** Western blot analysis of GLI processing in unstimulated and SAG-stimulated RPE1 cells with and without ADAMTS9 knockdown.

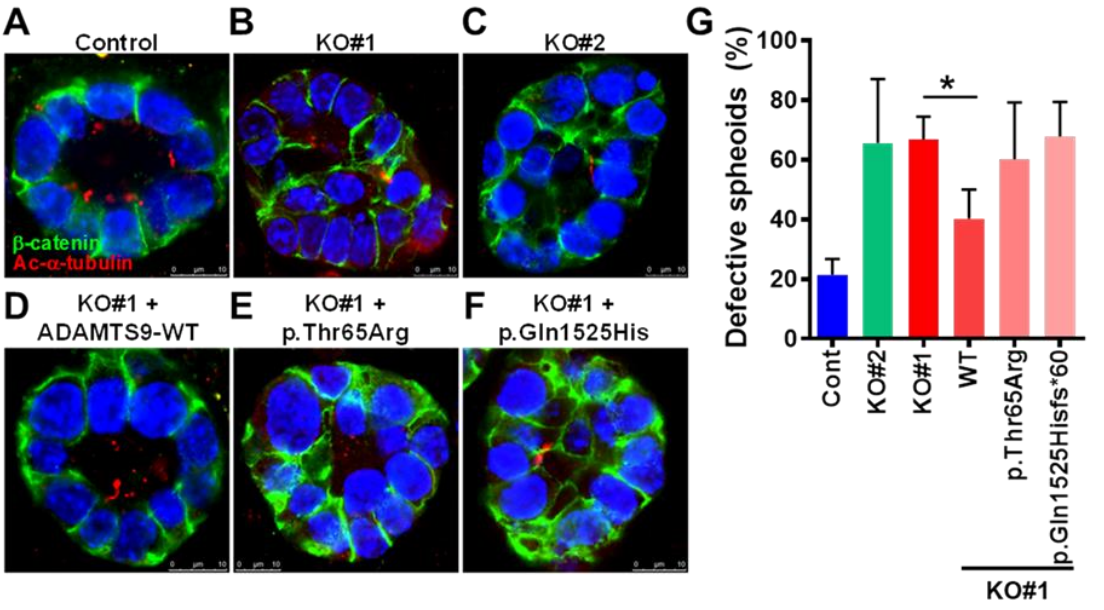

Figure 6. Adamts9 knockout perturbs lumen formation in 3D spheroid culture. **(A)** Effect of Adamts9 knockout (KO) using CRISPR/Cas9 system on primary cilia in IMCD3 cells. The **(A-F)** IMCD3 cells are ciliated apically and form a spheroid containing a central lumen when cultured in 3D Matrigel. Lumen formation were perturbed in Adamts9 knockout (KO) cells. Defective lumen formation was partially rescued by transfecting with human wild type (WT) ADAMTS9 but not ADAMTS9 constructs harboring mutations detected in individuals with NPHP-RC. **(G)** Percentage of abnormal spheroids. More than 200 spheroids were examined in each experiment. Data represent the mean + standard deviation of five independent experiments. *P < 0.05, t-test.

5. adamts9 Knockdown Replicates Ciliopathy Phenotypes in Zebrafish

To further validate the causative roles of ADAMTS9 mutations in the NPHP-RC phenotypes, we performed knockdown of the ADAMTS9 ortholog in zebrafish. We used translation-blocking (AUG) and exon 3 splice donor (e3i3) antisense morpholinos (MOs). The efficiency of the e3i3 MO was confirmed by RT-PCR, which demonstrated deletion of exon 3 (Figure 7A). Knockdown of adamts9 in zebrafish replicated characteristic ciliopathy phenotypes[24], including a ventrally curved body axis, hydrocephalus, or pronephric cysts at 3 days post-fertilization (dpf) (Figures 7B and 7C). Approximately 60%ofmorphants showed single or multiple ciliopathy phenotypes (Figure 7D), strongly suggesting that zebrafishadamts9 also has a role in primary cilium formation and function. Therefore, the role of ADAMTS9 in primary cilia seems to be evolutionarily conserved.

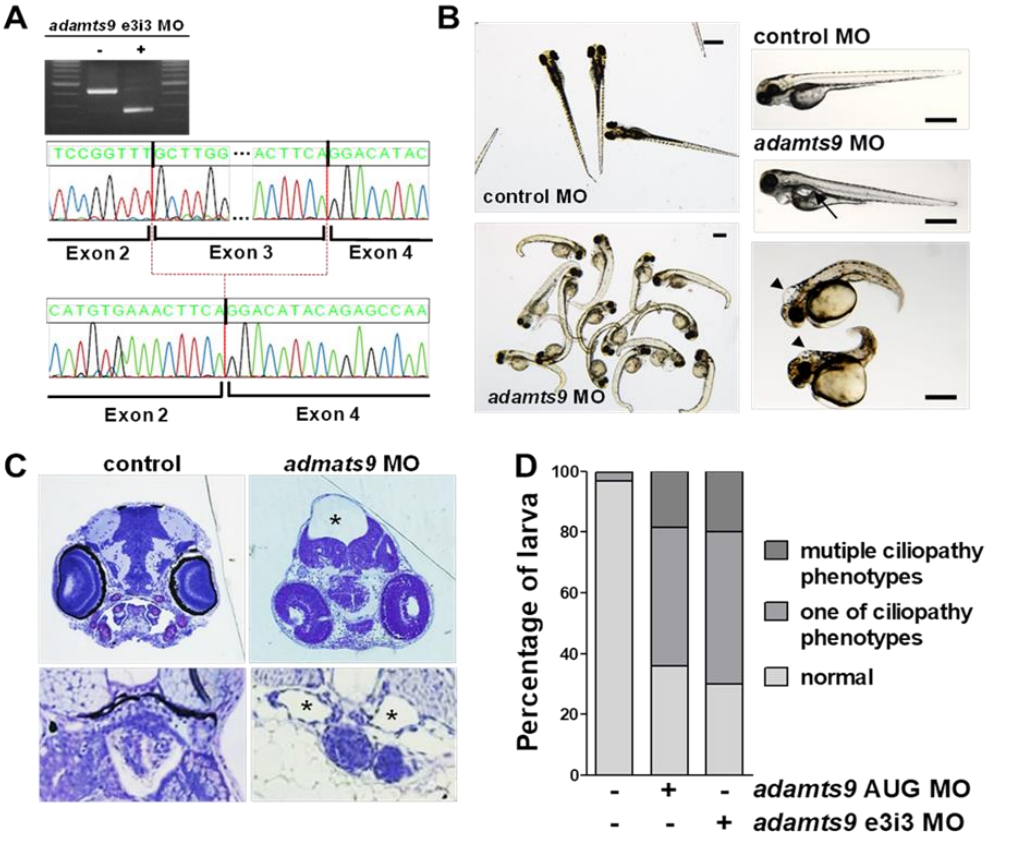

Figure 7. Knockdown of adamts9 in zebrafish recapitulates ciliopathy phenotypes. **(A)** RT-PCR shows that injection of e3i3 splice donor morpholino (MO) resulted in shortened adamts9 mRNA compared to wild type zmynd10 mRNA. Chromatogram of RT-PCR products revealed that exon 3 skipping was induced by e3i3 MO, resulting in splicing of exons 2 and 4 (i.e. exon 3 deletion). **(B)** Compared to control-injected embryos, embryos injected with either zmynd10-translation-blocking (AUG) or e3i3 MOs showed a ventrally bent body axis, pronephric cysts (arrows), and hydrocephalus(arrowheads). Scale bar is 100 mm. **(C)** Methylene blue staining showed hydrocephalus or dilation of the pronephric duct (asterisks) in adamts9 morphants. **(D)** Summary of phenotypes of zebrafish morphants. More than 200 larvae were counted per condition.

6. ADAMTS9 kidney organoids recapitulate ciliary defects

Kidney organoids have been used to model various genetic kidney diseases including nephronophthisis, a renal disorder resulting from defects in primary cilia. For example, Kidney organoids deficient for the ciliary transporter gene IFT140 exhibited abnormal ciliary morphology with swollen ciliary tip[25]. Here, we aimed to model ADAMTS9-related nephronophthisis in kidney organoids. We first investigated whether ADAMTS9 localized to peri-ciliary area in kidney organoids as well. In nephron organoids differentiated from induced pluripotent stem cells (iPSCs) using the protocol previously published by Taguchi et al.,[18] (Figure 8A). ADAMTS9 was observed near the basal bodies of primary cilia in tubules of kidney organoids. In particular, ADAMTS9 was co-localized with PCM-1, but did not completely overlap with γ-tubulin, confirming the peri-ciliary localization of ADAMTS9 (Figure 8B). To explore the effects of ADAMTS9 in kidney organoids, we generated iPSC clones in which ADAMTS9 was knocked out via CRISPR/Cas9 system (Figure 8C). Two ADAMTS9 knockout (KO) iPSCs, KO#1 and KO#2, were confirmed by Sanger sequencing of the exon 2 of the ADAMTS9 locus (Figure 8D). All three genotypes (WT, KO#1, and KO#2) were comparable upon differentiation, indicating that ADAMTS9 mutation did not affect differentiation of iPSCs into nephron progenitors. On day 32 of culture, all clones of the three genotypes differentiated into nephron organoids to form glomeruli (NEPHRIN+), and proximal (LTL+) and distal (CDH1+) tubules (Figure 8E and 8F). The proportion of glomeruli was higher in KO organoids compared to wild type organoids; however, this needs further examination (Figure 8E). As we have shown in multiple cell lines and zebrafish, primary cilia were also shortened or absent in tubular epithelia in kidney organoids differentiated from ADAMTS9 KO iPSCs (Figure 8G-I). Taken together, ADAMTS9-deficient nephron organoids recapitulates ciliary defects.

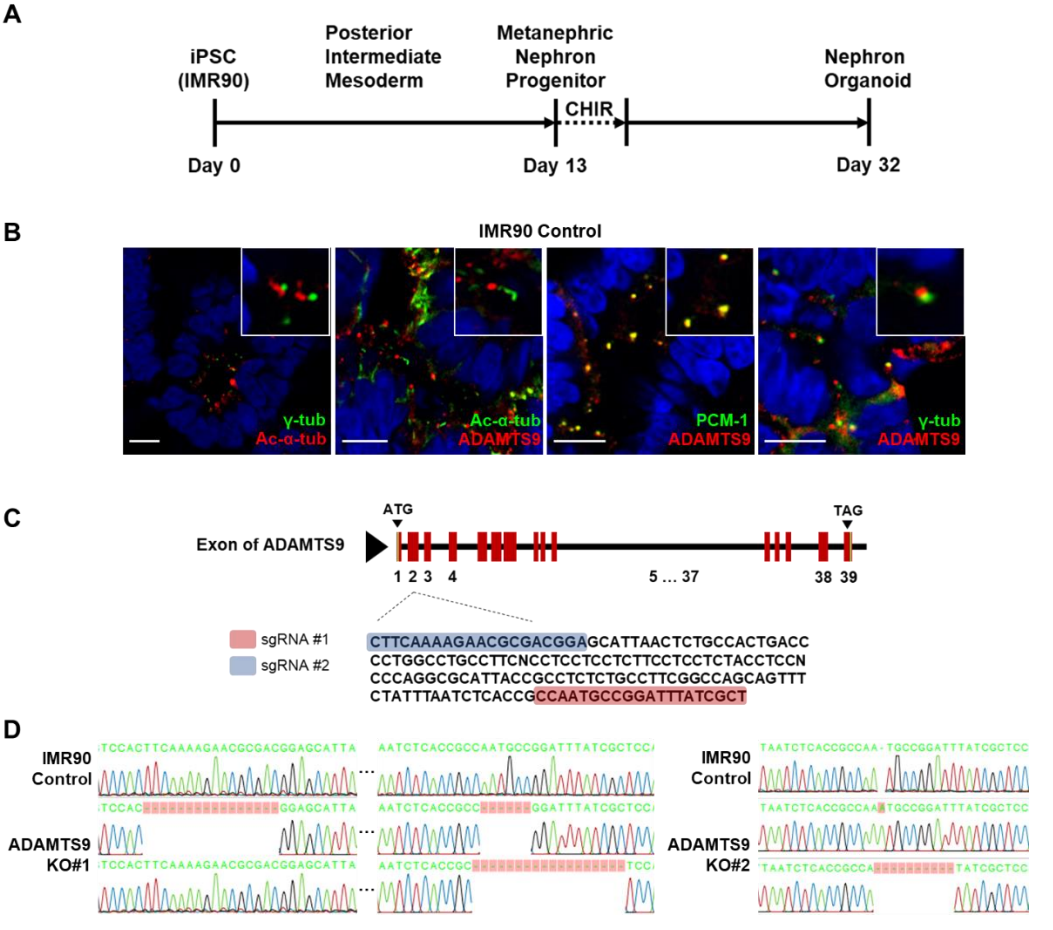

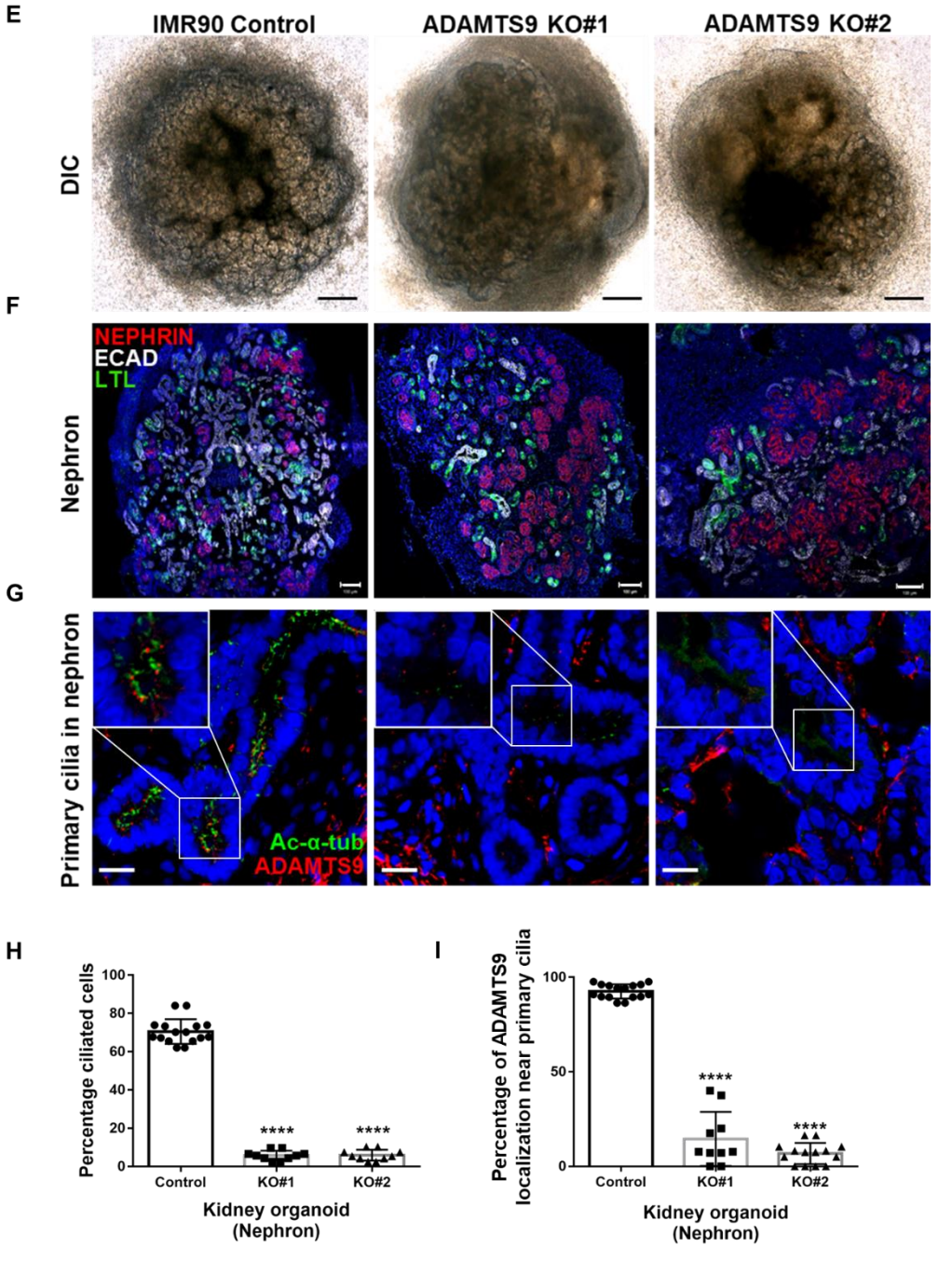

Figure 8. ADAMTS9 mutant nephron organoids exhibit ciliary defects. (A) Schematic of differentiation protocol for nephron organoids. **(B)** Immunofluorescence of wild-type nephron organoids at day 32 of differentiation. Organoids were stained with anti-γ-tubulin (γ-tub), anti-acetylated-α-tubulin (ac-α-tub), anti-ADAMTS9, and anti-pericentriolar material 1 (PCM-1) antibodies. Scale bars, 10 μm. (**C)** ADAMTS9 mutant iPSCs were generated using CRISPR/Cas9 system. Two sgRNAs, which targets the exon 2 of ADAMTS9, are indicated in colors. **(D)** Sanger sequencing of the exon 2 of ADAMTS9 confirmed genome editing in knockout (KO) iPSCs (KO#1 and KO#2). **(E)** Representative bright-field images of nephron organoids on day 32 of culture. Scale bars, 200 μm. **(F)** Immunofluorescence analysis of nephron segment-specific markers in kidney organoids at day 32. Nephron segments of the glomeruli (NEPHRIN; red), proximal tubules (LTL+; green), and distal tubules (ECADHERIN; white) were not different between wild-type and KO nephron organoids. Scale bars, 100 μm. **(G)** Anti-acetylated-α-tubulin staining demonstrated that primary cilia were deficient in ADAMTS9 KO organoids Scale bars, 20 μm **(H)** Percentage of ciliated cells. Experiments were repeated more than three times independently, and more than 200 cells were counted in each experiment. Data represent means ± standard deviation (SD). *$p < 0.05$, t test. **(I)** Percentage of cells with peri-ciliary localization of ADAMTS9. Experiments were repeated more than three times independently, and more than 100 cells were counted in each experiment.

IV. DISCUSSION

In this study, we reported novel homozygous and compound-heterozygous variants in ADAMTS9 identified in a family with NPHP-RC including multiple congenital birth defects. Our functional study of the identified variants showed that the mutations caused failure in localization of ADAMTS9 near into the vicinity of the basal body of the primary cilia. The p.Cys1024* and p.Q1525Hfs*60, nonsense variants, resulted in a truncated protein with complete loss of the GON domain, which is essential for endocytosis of ADAMTS9[12], thereby the resulting protein cannot undergo endocytosis and localize near basal bodies. In contrast, p.Ser636Phe, a missense mutation in the disintegrin-like domain (Figure 1J), was hypomorphic in the localization to the base of the primary cilia, but it is not clear how this variant causes the partial defect in localization. However, all identified variants in ADAMTS9 share the pathogenic mechanism of failure in trafficking of ADAMTS9 near basal bodies of primary cilia, stressing that its ciliary localization is essential for the function.

ADAMTS9 and a homolog, ADAMTS20, have a striking resemblance to their C. elegans ortholog, GON-1[7,26,27]. These proteases are members of a large secreted zinc metalloprotease family, whose members play diverse roles in tissue morphogenesis and human genetic and acquired conditions[28]. Members of the family share several distinct protein modules, including a propeptide, a metalloproteinase domain, a disintegrin-like domain, and thrombospondin type 1 motifs[28]. ADAMTS9 and GON-1 share a unique C-terminal domain called the GON-1 domain[26]. The proteoglycans aggrecan and versican are known substrates of ADAMTS9, and Adamts9-/- mice die during early gestation[13]. The four individuals with recessive ADAMTS9 mutations in this study presented with early-onset ESRD resulting from NPHP; proteinuria; deafness; short stature; and developmental delay. However, some clinical features differed between the each cases; for example, individual F1279-21 had developmental brain defects, but individual A5048-21 did not. Broad pleiotropy is a common feature of NPHP-RC, and mutations in the same gene can give rise to diverse phenotypes depending on the mutated allele[3]. In addition, modifier alleles can influence phenotypic expressivity, such

as when retinopathy manifests in individuals who have recessive NPHP1 mutations and also carry a heterozygous AHI mutation[29]. Individual F1279-21 had a homozygous frameshift mutation that resulted in a truncated protein with loss of both several thrombospondin motifs and the GON domain. In light of the fact that Adamts9-/- mice are embryonic lethal[13], null mutations might result in Meckel-Gruber syndrome (MIM: 249000) or disease phenotypes that are incompatible with life. Therefore, the frameshift mutation detected in individual F1279-21 is unlikely to be functionally null but rather is likely to be a hypomorph because the resulting truncated protein would retain the intact metalloproteinase activity. In this study, we showed that ADAMTS9 was present intracellularly near the base of the primary cilium during interphase. Because ADAMTS9 has a signal peptide and is conventionally transported through the endoplasmic reticulum to the Golgi apparatus and then to the extracellular space[26], the intracellular localization of ADAMTS9 to the base of the cilium was unexpected. This localization seems to be important for the ciliary function of ADAMTS9; the mutant ADAMTS9 proteins detected in individuals with NPHP-RC failed to localize to the base of the primary cilium and also failed to rescue defects in lumen formation. In addition, because treatment of cells with an endocytosis inhibitor prevented exogenous ADAMTS9 from reaching the base of the cilium, we concluded that endocytosis was required for localization of ADAMTS9 near basal bodies. These findings suggest that secreted ADAMTS9 needs to be endocytosed in order for it to be localized near the basal body. Additional research is necessary to reveal the machinery involved in the endocytic mechanism of ADAMTS9 and elucidate the pathway by which it reaches primary cilia. ADAMTS9 is a metalloprotease that regulates the structure and function of the extracellular matrix (ECM)[28]. In this study, we found that the loss of ADAMTS9 resulted in shortened cilia and defective Shh signaling, but it is not clear whether the metalloproteinase activity of ADAMTS9 is required for its ciliary function. It is known that the ECM can affect primary cilia formation and function[30], and renal cystogenesis is controlled by stromal composition[31]; therefore, it is plausible that shortened cilia might be due to ECM changes resulting from the loss of ADAMTS9. However, because we found that mutant ADAMTS9 proteins that retained the metalloproteinase domain

were secreted into the medium to the same extent as wild-type protein, the ECM is unlikely to differ in individuals with ADAMTS9 mutations. Rather, the intracellular function of ADAMTS9 near the basal body seems more relevant for primary-cilia function. However, it is not known whether ADAMTS9 detected near the basal body retains its metalloproteinase activity, and this also requires further investigation. In addition, there are 19 members in the human ADAMTS family[28]. ADAMTS9 belongs to the aggrecanase and proteoglycanase subgroup, which also includes ADAMTS1, 4, 5, 6, 15, and 20[28]. Thus, it will be interesting to examine whether any other ADAMTS proteins are involved in NPHP-RC.

V. CONCLUSION

In this study, we reported novel homozygous and compound-heterozygous mutations in ADAMTS9 identified in a family with multiple congenital defects. The mutations in ADAMTS9 identified as one of the causative genes of ciliopathy, which is a group of genetic disorders associated with defects in structure and function of primary cilia. Our functional study showed that all mutations caused failure in localization of ADAMTS9 near into the vicinity of the basal body of the primary cilia. Knockout of Adamts9 in a renal tubular cell line resulted in defective lumen formation upon spheroid induction, which was rescued by overexpression of wild-type, but not mutant ADAMTS9. Knockdown of adamts9 in zebrafish recapitulated NPHP-RC phenotypes, including renal cysts and hydrocephalus. We also established ADAMTS9 knockout human induced pluripotent stem cells by using CRISPR/Cas9 and differentiated into kidney organoid. We found ciliary defects in kidney organoid with deletion of ADAMTS9. Therefore, our identified mutations in ADAMTS9 share the pathogenic mechanism of failure in trafficking of ADMATS9 near basal bodies of primary cilia, suggesting that its ciliary localization is essential for the function.

REFERENCES

1. Hildebrandt F, Otto E. Hildebrandt, F. Otto, E. Cilia and centrosomes: a unifying pathogenic concept for cystic kidney disease? Nat. Rev. Genet. 6, 928-940. Nature reviews. Genetics 2006;6:928-40.
2. Reiter JF, Blacque OE, Leroux MR. The base of the cilium: roles for transition fibres and the transition zone in ciliary formation, maintenance and compartmentalization. EMBO reports 2012;13:608-18.
3. Braun DA, Hildebrandt F. Ciliopathies. Cold Spring Harbor perspectives in biology 2017;9:a028191.
4. Waters AM, Beales PL. Ciliopathies: an expanding disease spectrum. Pediatric nephrology (Berlin, Germany) 2011;26:1039-56.
5. Hildebrandt F, Zhou W. Nephronophthisis-associated ciliopathies. J Am Soc Nephrol 2007;18:1855-71.
6. Braun DA, Hildebrandt F. Ciliopathies. Cold Spring Harb Perspect Biol 2017;9.
7. Mead TJ, Apte SS. ADAMTS proteins in human disorders. Matrix Biology 2018;71-72:225-39.
8. Rim JH, Choi YJ, Gee HY. Genomic Landscape and Mutational Spectrum of ADAMTS Family Genes in Mendelian Disorders Based on Gene Evidence Review for Variant Interpretation. Biomolecules 2020;10.
9. Shiomi T, Lemaître V, D'Armiento J, Okada Y. Matrix metalloproteinases, a disintegrin and metalloproteinases, and a disintegrin and metalloproteinases with thrombospondin motifs in non-neoplastic diseases. Pathology international 2010;60:477-96.
10. Nandadasa S, Nelson CM, Apte SS. ADAMTS9-Mediated Extracellular Matrix Dynamics Regulates Umbilical Cord Vascular Smooth Muscle Differentiation and Rotation. Cell reports 2015;11:1519-28.
11. Choi YJ, Halbritter J, Braun DA, Schueler M, Schapiro D, Rim JH, et al. Mutations of ADAMTS9 Cause Nephronophthisis-Related Ciliopathy. Am J Hum Genet 2019;104:45-54.
12. Nandadasa S, Kraft CM, Wang LW, O'Donnell A, Patel R, Gee HY, et al. Secreted metalloproteases ADAMTS9 and ADAMTS20 have a non-canonical role in ciliary vesicle growth during ciliogenesis. Nature Communications 2019;10:953.

13. Dubail J, Aramaki-Hattori N, Bader HL, Nelson CM, Katebi N, Matuska B, et al. A new Adamts9 conditional mouse allele identifies its non-redundant role in interdigital web regression. Genesis 2014;52:702-12.
14. Kern CB, Wessels A, McGarity J, Dixon LJ, Alston E, Argraves WS, et al. Reduced versican cleavage due to Adamts9 haploinsufficiency is associated with cardiac and aortic anomalies. Matrix Biol 2010;29:304-16.
15. Garreta E, Prado P, Tarantino C, Oria R, Fanlo L, Martí E, et al. Fine tuning the extracellular environment accelerates the derivation of kidney organoids from human pluripotent stem cells. Nat Mater 2019;18:397-405.
16. Gee HY, Otto EA, Hurd TW, Ashraf S, Chaki M, Cluckey A, et al. Whole-exome resequencing distinguishes cystic kidney diseases from phenocopies in renal ciliopathies. Kidney Int 2014;85:880-7.
17. Giles RH, Ajzenberg H, Jackson PK. 3D spheroid model of mIMCD3 cells for studying ciliopathies and renal epithelial disorders. Nat Protoc 2014;9:2725-31.
18. Taguchi A, Nishinakamura R. Higher-Order Kidney Organogenesis from Pluripotent Stem Cells. Cell Stem Cell 2017;21:730-46.e6.
19. Halbritter J, Porath JD, Diaz KA, Braun DA, Kohl S, Chaki M, et al. Identification of 99 novel mutations in a worldwide cohort of 1,056 patients with a nephronophthisis-related ciliopathy. Hum Genet 2013;132:865-84.
20. Hildebrandt F, Benzing T, Katsanis N. Ciliopathies. N Engl J Med 2011;364:1533-43.
21. Corbit KC, Aanstad P, Singla V, Norman AR, Stainier DY, Reiter JF. Vertebrate Smoothened functions at the primary cilium. Nature 2005;437:1018-21.
22. Nandadasa S, Nelson CM, Apte SS. ADAMTS9-Mediated Extracellular Matrix Dynamics Regulates Umbilical Cord Vascular Smooth Muscle Differentiation and Rotation. Cell Rep 2015;11:1519-28.
23. Wen X, Lai CK, Evangelista M, Hongo JA, de Sauvage FJ, Scales SJ. Kinetics of hedgehog-dependent full-length Gli3 accumulation in primary cilia and subsequent degradation. Mol Cell Biol 2010;30:1910-22.
24. Schueler M, Braun DA, Chandrasekar G, Gee HY, Klasson TD, Halbritter J, et al. DCDC2 mutations cause a renal-hepatic ciliopathy by disrupting Wnt signaling. Am J Hum Genet 2015;96:81-92.
25. Forbes TA, Howden SE, Lawlor K, Phipson B, Maksimovic J, Hale L, et al. Patient-iPSC-Derived Kidney Organoids Show Functional Validation of a Ciliopathic Renal

Phenotype and Reveal Underlying Pathogenetic Mechanisms. Am J Hum Genet 2018;102:816-31.

26. Somerville RP, Longpre JM, Jungers KA, Engle JM, Ross M, Evanko S, et al. Characterization of ADAMTS-9 and ADAMTS-20 as a distinct ADAMTS subfamily related to Caenorhabditis elegans GON-1. J Biol Chem 2003;278:9503-13.
27. Dubail J, Apte SS. Insights on ADAMTS proteases and ADAMTS-like proteins from mammalian genetics. Matrix Biol 2015;44-46:24-37.
28. Kelwick R, Desanlis I, Wheeler GN, Edwards DR. The ADAMTS (A Disintegrin and Metalloproteinase with Thrombospondin motifs) family. Genome Biol 2015;16:113.
29. Louie CM, Caridi G, Lopes VS, Brancati F, Kispert A, Lancaster MA, et al. AHI1 is required for photoreceptor outer segment development and is a modifier for retinal degeneration in nephronophthisis. Nat Genet 2010;42:175-80.
30. Seeger-Nukpezah T, Golemis EA. The extracellular matrix and ciliary signaling. Curr Opin Cell Biol 2012;24:652-61.
31. Cruz NM, Song X, Czerniecki SM, Gulieva RE, Churchill AJ, Kim YK, et al. Organoid cystogenesis reveals a critical role of microenvironment in human polycystic kidney disease. Nat Mater 2017;16:1112-9.

ABSTRACT (IN KOREAN)

ADAMTS9 돌연변이에 의해 유발되는 콩팥황폐증의 발생기전

< 지도교수 지 헌 영 >

연세대학교 대학원 의과학과

최 요 준

콩팥황폐증 (nephronophthisis)은 신장 상피 세포에 존재하는 일차 섬모 (primary cilia)의 이상에 의해 발생하는 섬모병증 (ciliopathy)의 일종이다. 돌연변이가 발생하여 콩팥황폐증을 일으키는 원인유전자로 지금까지 90개이상의 유전자가 보고되었는데, 이들은 전체 콩팥황폐증의 50~60%를 설명할 수 있는 것으로 알려져 있다. 기존에 보고된 유전자로 해결되지 않은 콩팥황폐증 환자 샘플을 대상으로 Whole exome sequencing (WES)을 수행하였고, 4명의 환자에서 ADAMTS9의 돌연변이를 발견하였다. 이 환자들은 유아 및 소아에서 발생하는 만성 신부전증과 콩팥황폐증의 질환을 가졌고, 그밖에 짧은 신장, 난청, 성장 지연 등의 신장 외 다양한 증상을 나타내었다. ADAMTS9은 보통 세포 내 소포체 (vesicle)에 존재하거나 세포 밖으로 분비되어 세포 외 기질을 절단하는 메탈로프로테아제 (metalloprotease)의 기능을 가졌다고 알려졌으나, 우리는 세포 주기 간기 동안 ADAMTS9이 일차 섬모의 기저에 있는 basal body 근처에 존재하는 것을 확인하였다. 또한, ADAMTS9의 기능이 없어지면 일차 섬모의 길이가 짧아지고, 일차 섬모를 통해 매개되는 대표적 신호 체계인 Sonic hedgehog (Shh)의 활성이 감소함을 발견하였다. 본 연구에서 발견한 4개의 ADAMTS9돌연변이 (p.T65R, p.Q1525Hfs*60, p.C1024*, and p.S636F)는 일차 섬모 기저에 위치하지 못한다는 사실을

발견 할 수 있었다. 마우스 신장 상피 유래 세포(IMCD3)에서 Adamts9을 knockout 시키면, Spheroid 를 유도 시에 lumen 의 형성에 결함이 생기게 된다. 이러한 결함을 Wild-type 의 과발현(overexpression)으로 rescue 할 수 있었지만, mutant 로는 rescue 할 수 없었다. Zebrafish 에서 adamts9을 knockdown 시키면 renal cyst 와 hydrocephalus 등의 사람에서 나타나는 콩팥황폐증의 증상을 재현할 수 있었다. 마지막으로 인간 유도만능줄기세포(hiPSC)에 ADAMTS9 유전자를 CRISPR/Cas9시스템으로 knockout 을 시킨 후에, 신장 오가노이드로의 분화를 진행하였다. ADATMS9의 기능이 상실된 신장 오가노이드에서는 섬모 결함을 발견할 수 있었다. 본 연구를 통해서 ADAMTS9의 돌연변이가 섬모병증의 일종인 콩팥황폐증을 일으키는 것을 밝혔을 뿐만 아니라, ADAMTS9이 일차 섬모의 기능과 형성에 중요한 역할을 한다는 것을 밝혔다.

핵심되는 말: 콩팥황폐증, 섬모병증, ADAMTS9, 메탈로프로테아제, 일차 섬모, 신장 오가노이드

PUBLICATION LIST

1. **Yo Jun Choi**, Jan Halbritter, Daniela A. Braun, Markus Schueler, David Schapiro, John Hoon Rim, Sumeda Nandadasa, Won-il Choi, Eugen Widmeier, Shirlee Shril, Friederike Ko¨rber, Sidharth K. Sethi, Richard P. Lifton, Bodo B. Beck, Suneel S. Apte, Heon Yung Gee,1,* and Friedhelm Hildebrandt2,* Mutations of ADAMTS9 Cause Nephronophthisis-Related Ciliopathy. *The American Journal of Human Genetics.* 2019;104:45-54.
2. John Hoon Rim, **Yo Jun Choi**, Heon Yung Gee. Genomic Landscape and Mutational Spectrum of ADAMTS Family Genes in Mendelian Disorders Based on Gene Evidence Review for Variant Interpretation. *Biomolecules*. 2020 Mar 13 ; 10(3):449.